



**ILJS-19-012**

## **Influence of synthesis parameters on the morphology, purity and phases type of Copper oxide nanoparticles**

**Sanni<sup>1</sup>, H., Popoola<sup>1</sup>, A. S., Tijani<sup>1\*</sup>, J. O., Jacob<sup>1</sup>, J. O., Bankole<sup>1,3</sup>, M. T., Abdulkareem<sup>1,3</sup>, A. S.**

<sup>1</sup>Chemistry Department, Federal University of Technology, Minna, Niger State, Nigeria.

<sup>2</sup>Chemical Engineering Department, Federal University of Technology, Minna, Niger State, Nigeria.

<sup>3</sup>Nanotechnology Research Group, Centre for Genetic Engineering and Biotechnology, Federal University of Technology, Minna, Niger State, Nigeria.

### **Abstract**

In this study, copper oxide nanoparticles were synthesised by interaction of copper salt precursors with aqueous leaves extract of *Khaya senegalensis*. The influence of synthesis parameters such as solution pH (5, 9, 11, 13), copper salt types (chloride, nitrate and sulphate), calcination temperature (300°C – 500°C) and holding time (1-3 h) on the morphology and phase structure of CuO nanoparticles were examined. The as-synthesised materials were characterized by Energy Dispersive Microscopy (EDS), High Resolution Scanning Electron Microscope (HRSEM), Brunauer Emmett Teller (BET) N<sub>2</sub> adsorption-desorption technique, X-ray Photoelectron Spectroscopy (XPS) and X-ray Diffraction (XRD). The HRSEM/XRD analysis of the calcined CuO nanoparticles confirmed the formation of spherical and crystalline stable tenorite phase at optimum calcination temperature (550°C), and optimum holding time (3 h), pH (11) using copper sulphate salt precursors except for cupric acetate with no defined shape at pH of 7 and 13. BET analysis revealed the formation of mesoporous material with surface area of 20.64 m<sup>2</sup>/g. XPS analysis demonstrated the existence of Cu in the oxidation state of +2. This study established that the size and phase of CuO nanoparticles were dependent on the nature of the copper salts precursor, solution pH, calcination temperature and holding time.

**Keyword:** Green approach, optimization, synthesis parameters, CuO nanoparticles, Phase types.

### **1. Introduction**

Copper oxide (CuO) nanostructures have attracted significant attention among researchers due to their wide range of applications as high-temperature superconductors, gas sensors, catalyst, giant magnet resistance materials, and solar energy transformation (Jaise *et al.*, 2018). Copper oxide is also a p-type semiconductor with a band gap energy of 1.7 eV and

---

\*Corresponding Author: Tijani, J. O.  
Email: [jimohtijani@futminna.edu.ng](mailto:jimohtijani@futminna.edu.ng)

in different phases namely; tenorite (CuO), cuprite or perenox (Cu<sub>2</sub>O), copper (III) oxide (Cu<sub>2</sub>O<sub>3</sub>), and Cu<sub>4</sub>O<sub>3</sub> (Paramelaconite) (Alabi *et al.*, 2013; Devasenan *et al.*, 2016). Among the various metal oxide nanoparticles, CuO remained most technologically advanced and economically attractive due to its simplicity, high stability, lower surface potential barrier and cost effectiveness compared to gold and silver (Anwaar *et al.*, 2016; Asemani and Anarjan, 2019; Devasenan *et al.*, 2016). CuO nanoparticles are stable over a wide range of pH and high temperatures and have been extensively utilized in field emitting, photocatalysis (Katwal *et al.*, 2015), production of lithium ion battery (Thi *et al.*, 2014) and gas sensing (Zhang *et al.*, 2011).

Different conventional chemical methods such as sol-gel (Etefagh *et al.*, 2013), ball milling, physical/chemical vapor decomposition, solvothermal, flame pyrolysis, photo deposition, magnetic spluttering, precipitation (Phiwdang *et al.*, 2013), hydrothermal synthesis (Outokesh *et al.*, 2011) have been utilized to produce CuO nanoparticles. Others include chemical reduction, thermal decomposition, electrochemical method (Ghorbani, 2014) and wet chemical method (Joshua *et al.*, 2014). These methods have certain shortcomings such as high cost of reagents, high energy requirement, time consumption, and complex synthesis procedures. The methods also employed toxic chemicals and generate toxic byproducts (Li *et al.*, 2011; Zhou *et al.*, 2010).

On the contrary, green synthesis using plant extracts or bacteria, fungi, human and animal cells, algae and others is simple, environmental friendly, and generate less toxic products than conventional methods (Umar *et al.*, 2009). The plant extracts reduce the metal ions from their various oxidation states to zero valent of the respective metals and the extracts also acts as stabilization and capping agent for the nanoparticles (Das *et al.*, 2013). Plant materials are readily available and abundant compared to commercial reductants such as LiAlH<sub>4</sub> and NaBH<sub>4</sub> that are toxic and expensive. In this study, the aqueous leaves extract of *Khaya senegalensis* commonly known as African mahogany, Senegal mahogany, *Khaya* wood or Gambia mahogany was used to prepare CuO nanoparticles. This is a medium sized tree that belongs to the order *Sapindales* and family *Meliaceae*. The plant grows between 15-30 m height and 1 m in diameter and commonly found in riparian forest and higher rainfall savannah woodlands of Benin, Cameroon, Burkina Faso, Nigeria, Togo, and Uganda. Studies conducted on the aqueous leave extract of the plant revealed the presence of flavonoids, glycosides, carbohydrates, saponins, tannins, alkaloids and anthraquinones (Marakov *et al.*,

2014). These phytochemical constituents make the leaves of *Khaya senegalensis* a good reducing agent to reduce copper salt into copper oxide nanoparticles.

Furthermore, different researchers namely; Jayalakshmi and Yogamoorthi, (2014) (aqueous flower extract of *Cassia alata*); Naika *et al.*, (2015) (*Gloriosa superba* leaf extract); Saeid and Ali (2016) (coffee powder extract), Sumitha *et al.*, (2016) (extract of *Ocimum tenuiflorum*), Anisilin *et al.*, (2016) (Neem leaf extract) have utilized different plant parts to prepare nano sized CuO of several phases, morphology and microstructures. For instance, Sharma *et al.* (2016) observed a phase transformation from malachite  $\text{Cu}_2(\text{CO}_3)(\text{OH})_2$  to tenorite with crystallite size increment from 36 nm to 76 nm respectively. Othmane *et al.* (2017) observed no weight loss for CuO nanoparticles calcined in the furnace below or above 500°C however found that crystallinity increased with increasing temperature from 400°C to 800°C. Siddiqui *et al.* (2016) investigated the effect of copper salt precursors (copper nitrate ( $\text{Cu}(\text{NO}_3)_2$ ), and copper chloride ( $\text{CuCl}_2$ )) on the shapes of CuO nanoparticles synthesized via hydrothermal method. XRD analysis revealed monoclinic phase of CuO nanocrystals while FESEM analysis of CuO prepared using  $\text{CuCl}_2$  precursor confirmed mixture of dense packed cubic and sphere shaped particles. While ( $\text{Cu}(\text{NO}_3)_2$ ) precursor showed only flakes like morphology.

Additionally, studies have shown that the crystallite size and shape largely depend on the method of synthesis, salt precursors and other applied experimental conditions. On the other hand, the effects of the synthesis parameters such as calcination temperature, copper salts precursor type, solution pH, calcination time on the morphology and phase types of CuO nanoparticles is yet to be reported. This study reports for the first time the green synthesis of copper oxide nanoparticles. The influence of solution pH, copper salts precursor, calcination temperature and holding time on the size, phase and shape of CuO nanoparticles were examined. The prepared CuO nanoparticles were characterized for their morphology, elemental composition, mineralogical phase, surface area and surface oxidation states of the elements using High Resolution Scanning Electron Microscope (HRSEM), Energy Dispersive Spectroscopy (EDS), X-ray Diffraction (XRD), Brunauer–Emmett-Teller ( $\text{N}_2$  BET) and X-ray Photoelectron Spectroscopy (XPS).

## 2. Materials and Methods

The following analytical grade chemicals: copper acetate monohydrate, copper (II) chloride dehydrate, copper sulphate, sodium hydroxide, and hydrochloric acid with percentage purity in the range of 95-99.8% were obtained from Sigma Aldrich and used without further purification.

### Sample Collection and Pretreatment

The leaves of *Khaya senegalensis* were randomly collected along Niger State Government house, Minna, Nigeria and subsequently washed properly with distilled water to remove any impurities and later air-dried for 10 days. The air-dried samples were then milled into powdery form using electric blender and then sieved with 2  $\mu\text{m}$  mesh to obtain homogenous size.

### Preparation of the Plant Extract

Twenty grams (20 g) of the powder plant sample was weighed and put into a 500  $\text{cm}^3$  beaker containing 400  $\text{cm}^3$  of distilled water. The mixture was stirred using a glass stirring rod and allowed to boil for about 25-30 minutes on a hot plate and later allowed to cool. The brownish mixture was filtered using Whatmann No 1 filter paper and the extract obtained was put in a conical flask and stored in a refrigerator maintained at 4°C for further use.

### Green synthesis of CuO nanoparticles

The green synthesis of CuO nanoparticle was carried out as follows: 1.2 g of cupric acetate ( $(\text{CH}_3\text{COO})_2\text{Cu}\cdot\text{H}_2\text{O}$ ) was weighed and dissolved in 20  $\text{cm}^3$  of distilled water followed by heating on magnetic stirrer at 150 rpm for 3 h until a blue colouration was obtained. To this solution, 50  $\text{cm}^3$  of extract was added under continuous stirring while 0.5 M NaOH solutions was added drop wise to adjust the pH to 10. The mixture was later stirred for 30 minutes and the appearance of dark green colouration indicated the formation of CuO nanoparticle. The mixture was allowed to settle after which the upper layer liquid was decanted and the precipitate (dark green) was washed severally with distilled water until a clear filtrate was obtained. The CuO nanoparticles formed were put in a crucible and dried in an oven at 80°C for 3 h. This procedure was repeated using 0.3 M of copper sulphate ( $\text{CuSO}_4$ ) and copper (II) chloride dihydrate ( $\text{CuCl}_2\cdot 2\text{H}_2\text{O}$ ) for the synthesis of CuO nanoparticles. For the variation of solution pH, the mixture of each copper salt precursor and aqueous leaves extract of *Khaya senegalensis* was later adjusted to 9, 11 and 13 using 1 M NaOH solution. The nanoparticles

formed under the applied conditions were centrifuged and the upper layer decanted while the lower layer was filtered using Whattman No. 1 filter paper.

### **Effect of Calcination Temperature and Calcination Time**

The effects of calcination temperature and time on the prepared CuO nanoparticles were studied by subjecting 3.5 g of the synthesized CuO nanoparticles produced to different calcination temperatures (300°C, 400°C, 500°C) and calcinations time (1, 2, 3 h) in a muffle furnace. At the end of each experiment, the crucible containing black solid residue of CuO nanoparticle was removed from the furnace and allowed to cool.

### **Characterization of the prepared CuO nanoparticles**

The morphology of the prepared CuO nanoparticles was determined using Zeiss Auriga High Resolution Scanning Electron Microscopy (HRSEM). The individual element in the samples was examined by energy dispersive spectroscopy via adjustment of the measurement angle of the detector. XRD instrument Bruker AXS Advanced diffractometer with Monochromatic Copper (Cu)-K $\alpha$  radiation, wavelength of 0.154 nm was used for phase structure identification, cell dimension, atomic spacing. The diffractograms were recorded with  $2\theta$  range of 20 - 90°, a step size of 0.028°, and operating at 45 kV and 40 mA was used to collect XRD data. The mean crystallite size of the nanoparticles (D), were obtained by means of the Debye-Scherrer's equation given as:

$$D = \frac{k\lambda}{\beta \cos\theta},$$

where k is a constant (k=0.94), and  $\lambda$  is wavelength = 0.1541 nm,  $\theta$  is Bragg angle and  $\beta$  the full width half maximum (FWHM) of the peak at  $2\theta$ . The surface area, pore volume and pore size distribution of the prepared samples were determined by Brunauer–Emmett-Teller (N<sub>2</sub> BET) adsorption-desorption technique using a NOVA 4200e surface area and pore analyzer instrument. The PHI 5400 XPS spectrometer using a non-monochromatic Mg K $\alpha$  X-ray source (1253.6 eV, 15 kV, 200 W) and hemispherical sector analyser was used to determine the surface oxidation states of the elements in the CuO nanoparticles. Spectra were analysed using XPS PEAK 4.1 software.

## **3. Result and Discussion**

## High Resolution Scanning Electron Microscopy (HRSEM) of Synthesized CuO Nanoparticles at different calcinations temperatures and holding time

HRSEM was utilized for the morphology of the synthesized CuO nanoparticles using copper acetate monohydrate precursor at different calcination temperatures of 300°C, 400°C and 500°C and holding time of 1, 2 and 3h and the results are shown in Figures 1- 3.

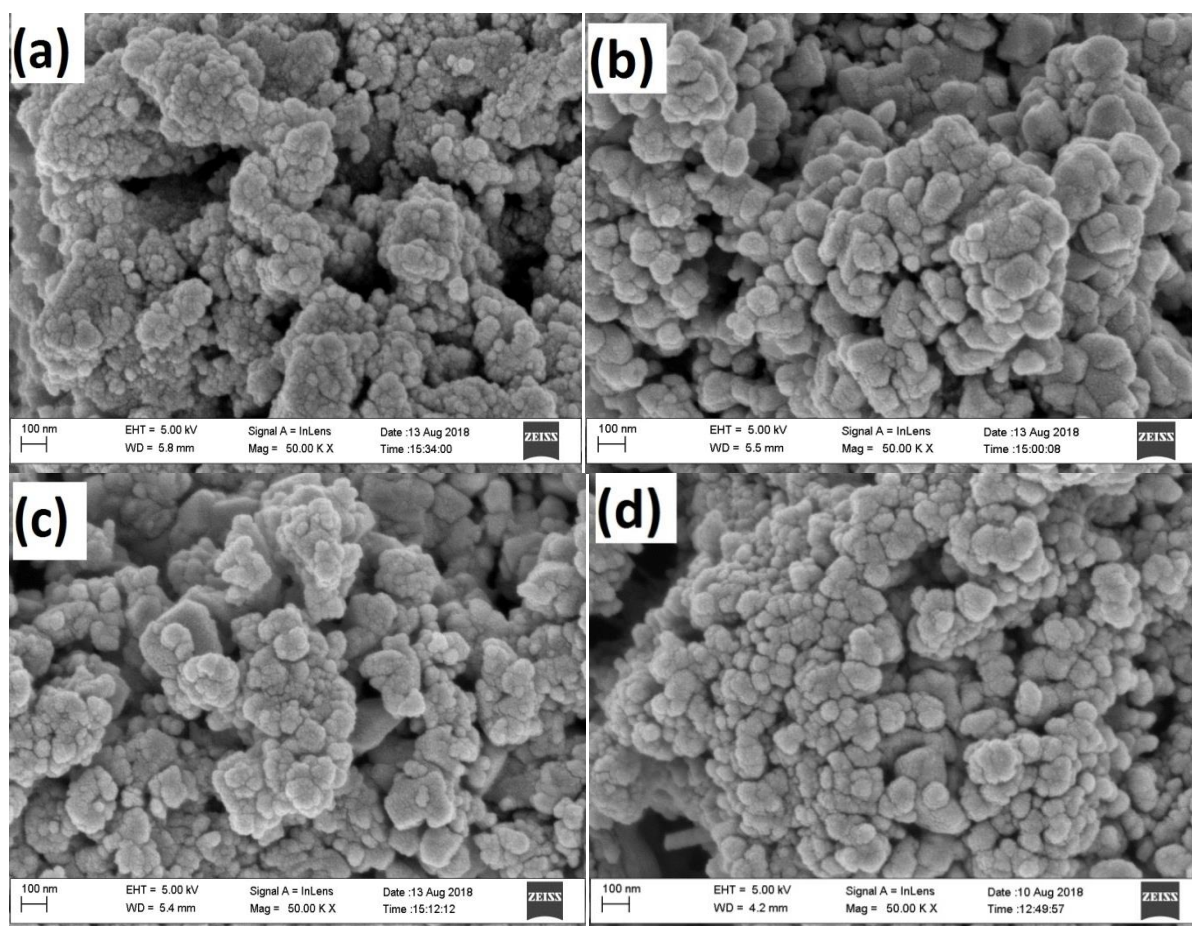


**Figure 1:** HRSEM image of synthesized CuO nanoparticles; (a) uncalcined and calcined at (b) 300°C for 1h, (c) 300°C for 2 h and (d) 300°C for 3 h.

It was observed from the HRSEM image in figure 1 (a) that the uncalcined CuO nanoparticles were agglomerated in nature. When the synthesized CuO nanoparticles were subjected to calcination temperature of 300°C at a holding time of 1 h, the particles became more dispersed and spherical in nature. At holding time of 2 h, the spherical symmetry became more distinct than the samples calcine at 1 h. At holding time of 3 h, the spherical symmetry become more defined and uniformly distributed which supports the findings of Naika *et al.* (2015) that demonstrated the formation of uniformly distributed spherical CuO

nanoparticles at calcination temperature of 300°C. At temperature of 400°C and holding time of 1 h (Figure 2 (a)), clustered CuO nanoparticles with a mixture of spherical and hexagonal shapes were observed.

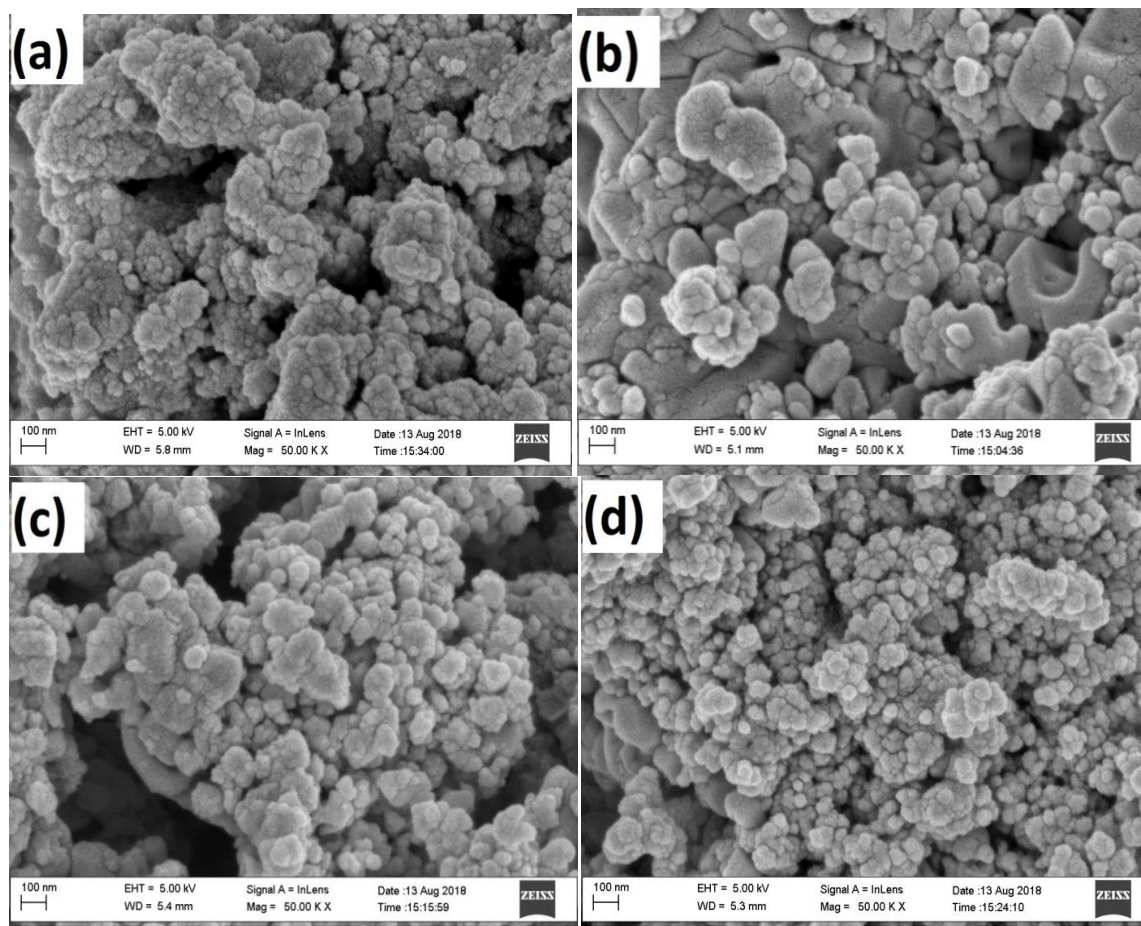


**Figure 2:** HRSEM image of synthesized CuO nanoparticles for (a) uncalcined and calcined at (b) 400°C for 1h, (c) 400°C for 2 h and (d) 400°C for 3 h

As the holding time was increased to 2 h, clearer, less agglomerated, purely spherical CuO nanoparticles were observed. At a holding time of 3 h, the CuO nanoparticle became less agglomerated and had more defined spherical shapes corresponding to a monoclinic phase. Similar observation was reported by Saeid and Ali (2016) in their study using coffee power extract and copper nitrate nonahydrate precursor. As the temperature was increased to 500°C, less agglomerated, purely spherical CuO nanoparticles were obtained (see Figure 3). The shape of CuO nanoparticles became more defined as the calcination time increases. The formation of well defined spherical shapes at this temperature and holding time was linked to capping and stabilization effect provided by the extract of *Khaya senegalensis*.

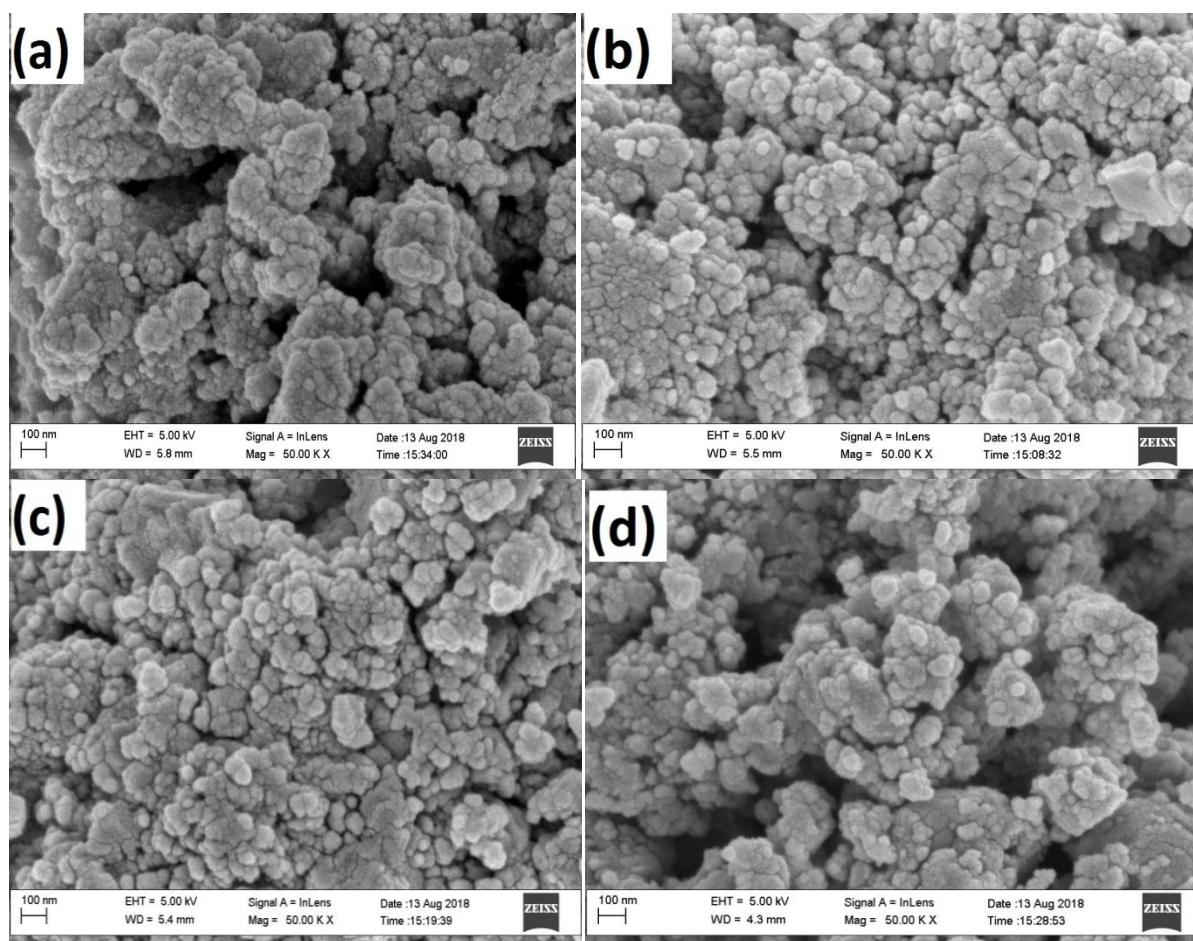


**Figure 3:** HRSEM image of synthesized CuO nanoparticles for (a) uncalcined and calcined at (b) 500°C for 1h, (c) 500°C for 2 h and (d) 500°C for 3 h

Comparatively, it was noticed that as the calcination temperature of the CuO nanoparticles increased from 300°C to 500°C, the morphological and structural arrangement also changed and the CuO nanoparticles with defined spherical shape were formed. The crystallization of CuO fairly improves as the calcination temperature and holding time increases. Additionally, the size of the CuO nanoparticles increased with increasing temperature. These findings are in agreement with previous studies reported by Koshi and George (2014) and Othmane *et al.* (2017) on the effect of calcination temperature on CuO nanoparticles.

### Energy Dispersive Spectrum of CuO Nanoparticles

The EDS analysis was done to investigate elemental composition of the uncalcined and calcined CuO nanoparticles prepared at different calcination temperatures and holding time and the result is shown in Table 1.

**Table 1:** Elemental Composition of Synthesized CuO Nanoparticles at different temperatures and holding time.

Samples	C	O	Na	Mg	Si	S	Ca	Cu
	(%)							
300°C 1h	10.64	27.69					2.44	59.23
2h	10.87	13.40					3.28	72.45
3h	10.01	11.24					3.26	75.49
400°C 1h	9.65	24.12					1.83	64.40
2h	10.68	15.63					2.10	71.59
3h	11.20	11.99					1.55	85.25
500°C 1h	10.38	20.43					3.47	65.72
2h	10.40	17.54					4.53	67.53
3h	10.47	10.03	1.12				3.98	74.40
Uncalcined	42.19	33.72					0.83	23.26

Table 1 shows the percentage composition of the elements present in the synthesized CuO nanoparticles which include copper, carbon, oxygen, sodium, magnesium, silicon, sulphur and calcium. It can be noticed that the dominant elements in the prepared material were copper and oxygen, which confirmed that the prepared materials is CuO nanoparticles. The reaction of copper salt precursors with the plant extract in the presence of NaOH as a precipitating agent initially yield  $\text{Cu}(\text{OH})_2$ , which further decompose during calcinations process at elevated temperature to give CuO nanoparticles according to equations 1 and 2:



While other elements were present as impurities either from the salt precursor used or due to improper washing. However, the carbon present could originate from two sources either from the carbon grids used during the analysis or the plant extracts used. The Na present in the samples originated from NaOH used for the adjustment of solution pH. A common trend was noticed for prepared CuO nanoparticles calcined at different calcination temperatures and holding time, the percentage of Cu present in the sample increases while oxygen content

reduced. On the other hand, the atomic percentage of Cu in the uncalcined sample was small while O content was slightly higher relative to the calcined samples at different temperatures. This may be due to the amorphous nature of materials prior to calcination. It was also noticed that as the calcination temperature and time increases, the oxygen content reduced while the atomic percentage of Cu increased. This was attributable to the removal of residual water from  $\text{Cu}(\text{OH})_2$  during the calcination process.

### High Resolution Scanning Electron Microscope (HRSEM) analysis of the prepared CuO nanoparticles at different solution pH and copper salt precursors

The HRSEM micrograph of CuO nanoparticles synthesized at different pH using cupric acetate is shown in Figure 4. It was observed from the figure that most of the particles were well dispersed and spherical in shape except the image shown in Figure 4 (d).

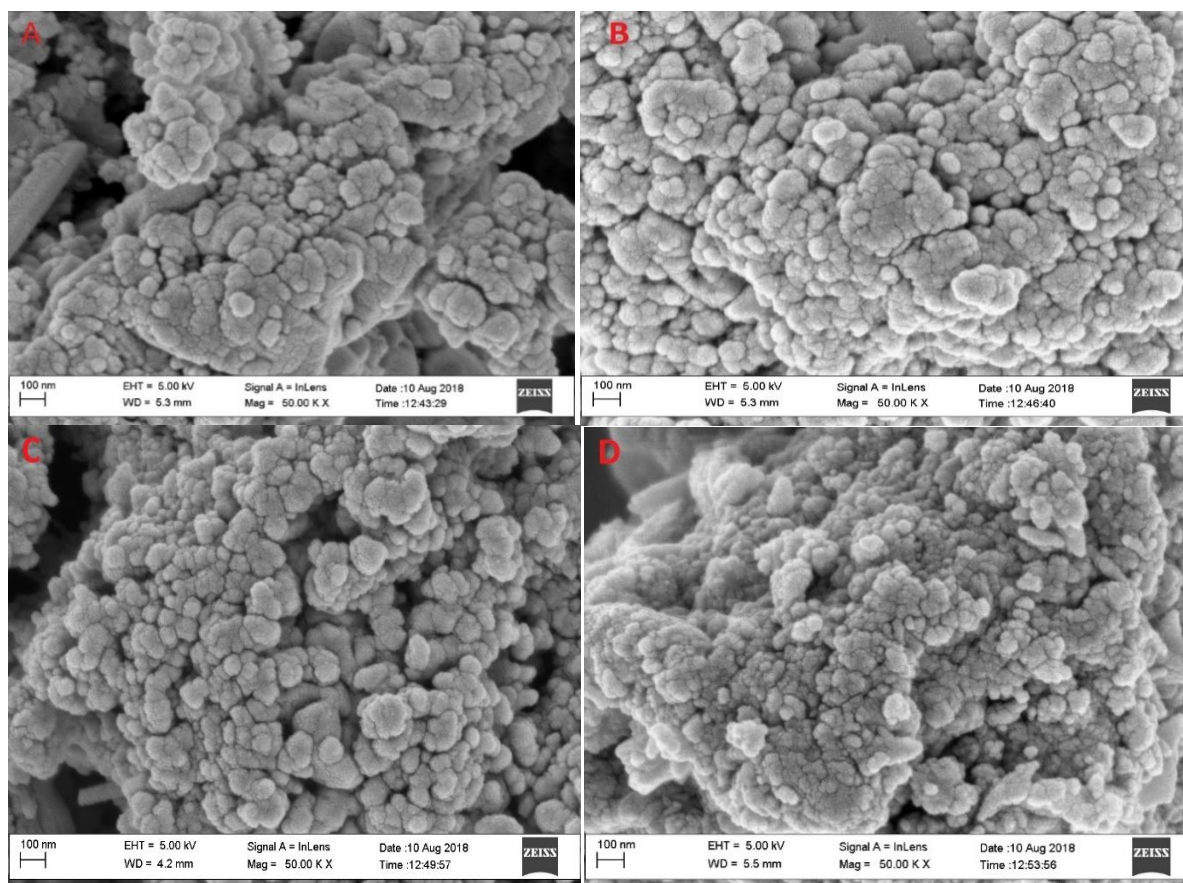


**Figure 4:** HRSEM images of CuO nanoparticles of cupric acetate at different pH value (a) 7 (b) 9 (c) 11 (d) 13.

It can be seen from Figure 4 (a) that at pH of 7, tiny spherical and sparsely distributed particles were formed. While at pH of 9, agglomerated closely packed spherical shaped particles with sizes bigger than that obtained at pH 7 were formed. The formation of

agglomerated particles may be linked to Ostwald ripening process. However at pH of 11, less agglomerated with clear porosity and homogeneous particles were observed. It was noticed that no visible particles were formed at pH 13. This implies that highly basic solution did not favour the growth of CuO nanoparticles. Also in Figure 5, it was noticed that at pH of 7, few spherical particles were formed when copper (II) chloride precursor was used. While at pH of 9, well distinct spherical shaped particles were formed. This may be ascribed to strong electrostatic attraction between the positive charged copper salt precursor and hydroxide ion in the solution. While at pH of 11 and 13, the particles formed were agglomerated with no definite shape. This phenomenon can be explained in terms of reduction of electrostatic interaction between hydroxide ions and copper salts precursor at pH beyond 9. During the experiment, it was found that acidic medium did not favour the formation of CuO nanoparticles. Not only that, high degree of alkalinity or basicity did not promote the growth and formation of well structured CuO nanoparticles. Similar trend was noticed in Figure 5 for pH 9 and 11.

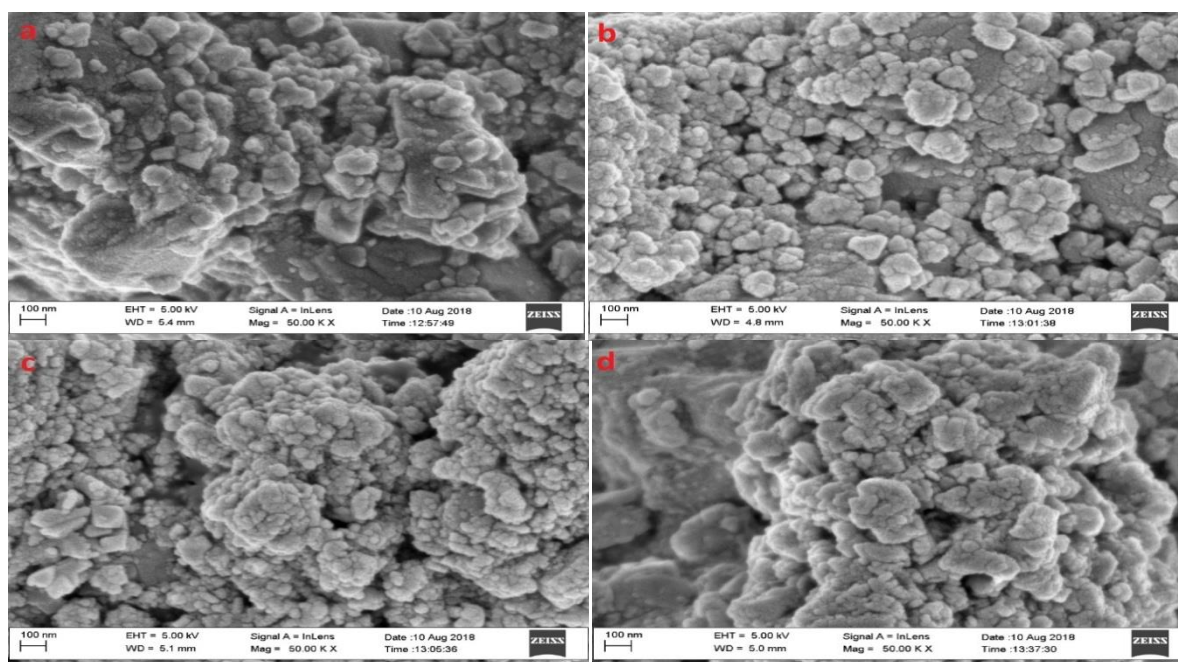


**Figure 5: HRSEM images of CuO nanoparticles of copper (II) chloride at different pH (a) 7 (b) 9 (c) 11 (d) 13**

As shown in Figure 6, it can be seen that at the pH of 7, the shape of the CuO nanoparticles were not well defined and the particles were agglomerated while at pH of 9, the particles were less compacted and more defined spherical shape were formed compared to pH of 7 were formed. While at pH of 11, well distinct and homogeneous spherical shaped particles

were formed. Comparatively, it can be observed that copper salt precursors and solution pH influenced the shape of the nanoparticles formed.

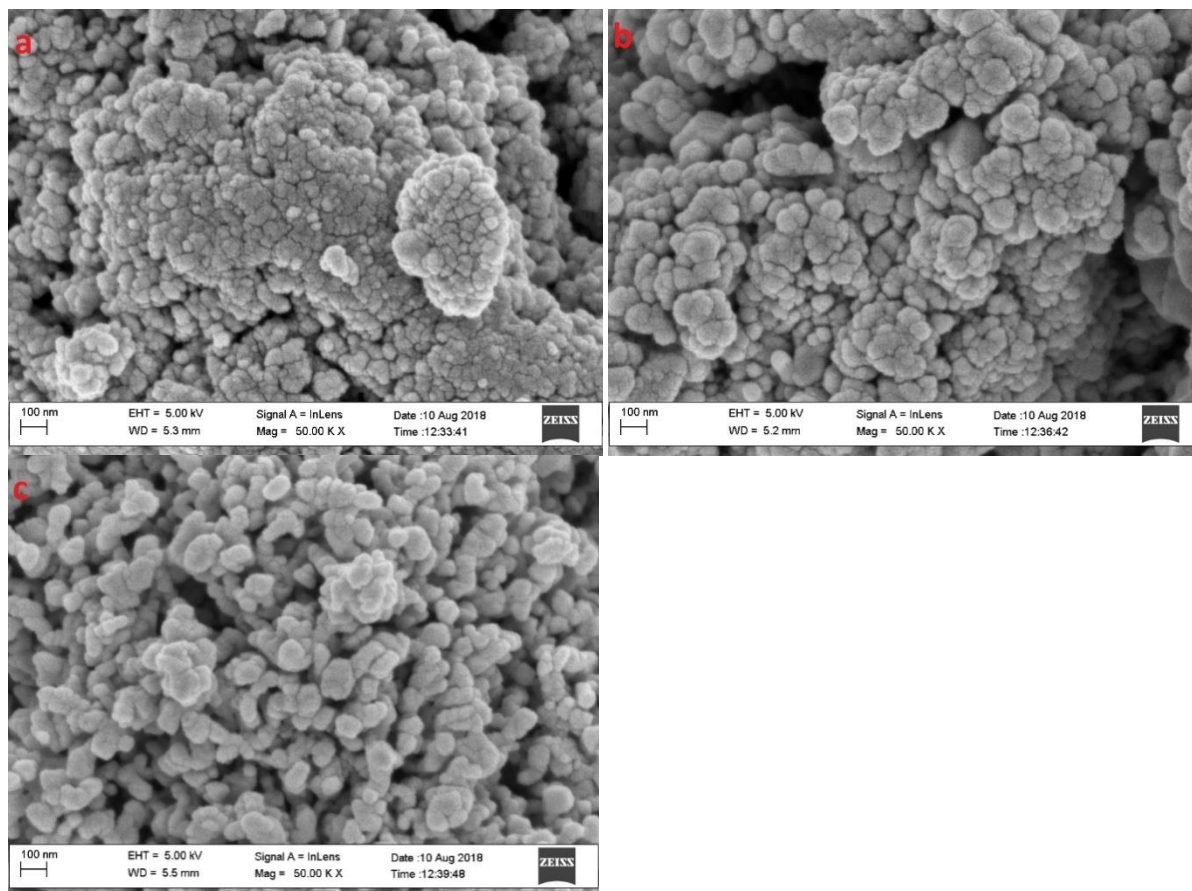


**Figure 6:** HRSEM images of CuO nanoparticles of copper sulphate at different pH (a) 7 (b) 9 (c) 11.

### **X-Ray Diffraction Analysis of synthesized CuO nanoparticles at different calcination temperature and holding time**

X-Ray diffraction (XRD) analysis was done to determine the crystal structure and the crystallite size of the synthesized CuO nanoparticles. The Debye-Scherrer's equation was used to estimate the crystallite size. The effects of calcination temperature and holding time on the particle size of the synthesized CuO nanoparticle were investigated. Figure 7 illustrates XRD diffraction patterns of CuO nanoparticles calcined at 300°C for holding time of 1, 2 and 3 h.

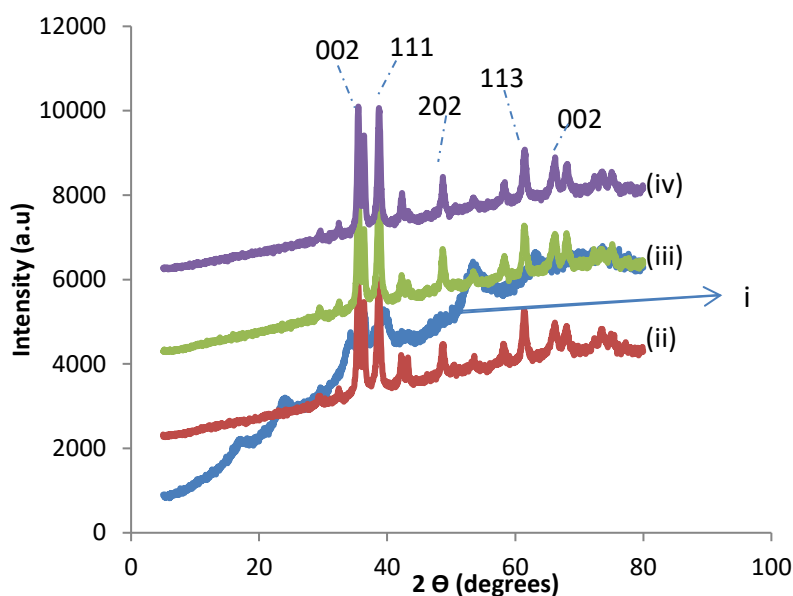
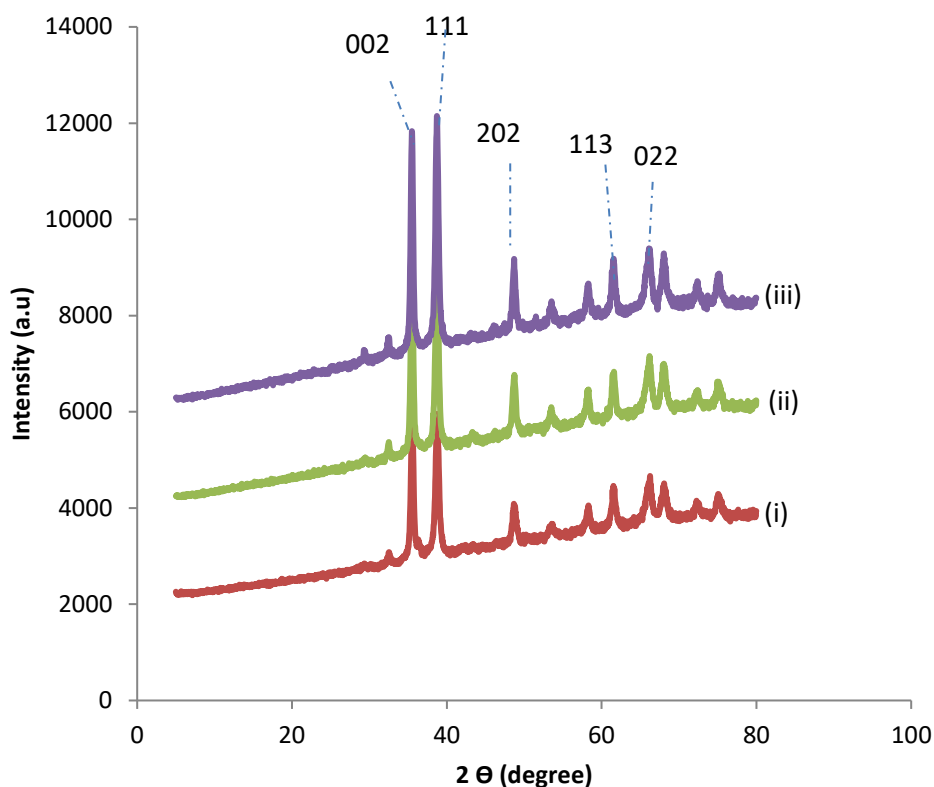


**Figure 7 (a):** X-ray Diffraction of (i) Uncalcined CuO Nanoparticles (ii) Calcined CuO Nanoparticles at 300°C for 1 h, (ii) 300°C for 2 h and (iii) 300°C for 3 h.

The XRD pattern of the CuO nanoparticles calcined at 300°C for 1, 2 and 3 h demonstrated the presence of five intense observable diffraction peaks at  $2\theta$  values of 34.91°, 38.65°, 48.56°, 61.26° and 65.89° with their corresponding crystal planes of (002), (111), (202), (113) and (002) respectively irrespective of the holding time. This corresponds to monoclinic tenorite phase. In the case of the uncalcined sample, low intense peaks were observed at  $2\theta$  values of 34.91° and 48.56°. The presence of peaks of low intensity suggests the amorphous nature of the sample, which is in good agreement with other works. It was also observed that as holding time increased, the peaks became more intense and the crystallite size increased in the order 3.43 nm < 6.77 nm < 7.82 nm for 1, 2 and 3 h respectively. The crystallites size reported in this study was less than 10 nm reported by Thekkae Padil and Černík, (2013) who prepared CuO nanoparticles via colloid-thermal synthetic method involving interaction of  $\text{CuCl}_2 \cdot 2\text{H}_2\text{O}$  and *Gum karaya*. The differences in size may be linked to the method of synthesis. It is noteworthy to mention that CuO nanoparticles formed irrespective of the holding time.

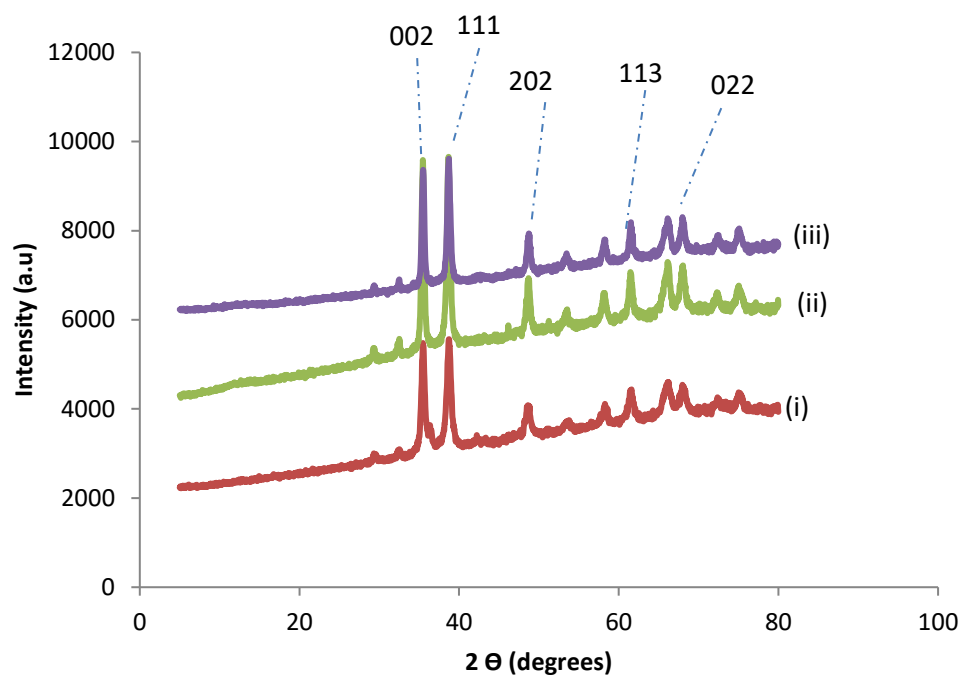
Similarly, the XRD diffraction pattern for the CuO nanoparticles calcined at 400°C (Figure 7 (b)), revealed the presence of five intense characteristic diffraction peaks at  $2\theta$  value of 35.43°, 38.65°, 48.60°, 61.26° and 65.65°. These correspond to monoclinic tenorite phase with the following crystal planes (002), (111), (202), (113) and (022). Again, it was noticed that

the intensity of the diffraction peaks increases with increasing holding time and crystallite size also increase in the order 4.24 nm < 6.09 nm < 7.38 nm for 1, 2 and 3 h respectively.



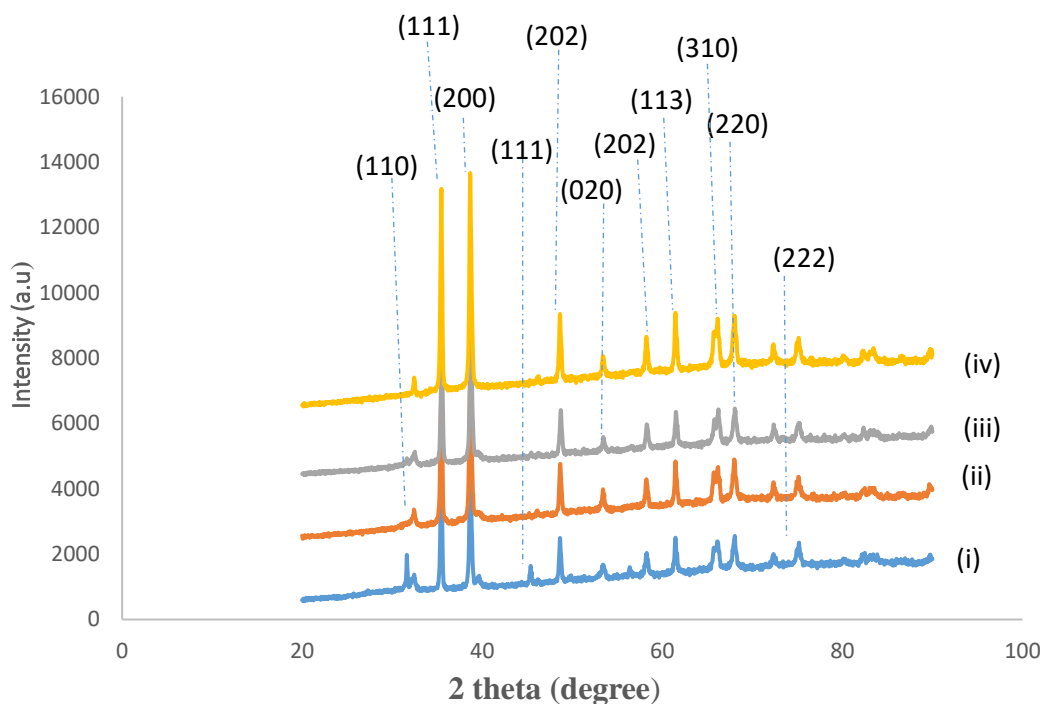
**Figure 7 (b):** X-ray Diffraction of CuO Nanoparticles calcined at 400°C for (i) 1 h, (ii) 2 h and (iii) 3 h.

Figure 7(c) shows the diffraction pattern of CuO nanoparticles calcined at constant temperature of 500°C and varying holding time of 1, 2 and 3 h. Again, five sharp and intense peaks were observed at  $2\theta$  values of  $35.746^\circ$ ,  $38.65^\circ$ ,  $48.56^\circ$ ,  $61.22^\circ$  and  $65.30^\circ$  corresponding to crystal indices of (002), (111), (202), (113) and (022). It is obvious that the increase in the holding time has a profound effect on the intensity of the peaks. The intensity of the peaks is directly proportional to the holding time, which suggests that holding time influences the crystallinity of the material. Crystallite size of the nanoparticles calcined at 500°C increase with increasing temperature in the order 8.09 nm < 9.26 nm < 11.12 nm for 1, 2 and 3 h respectively.



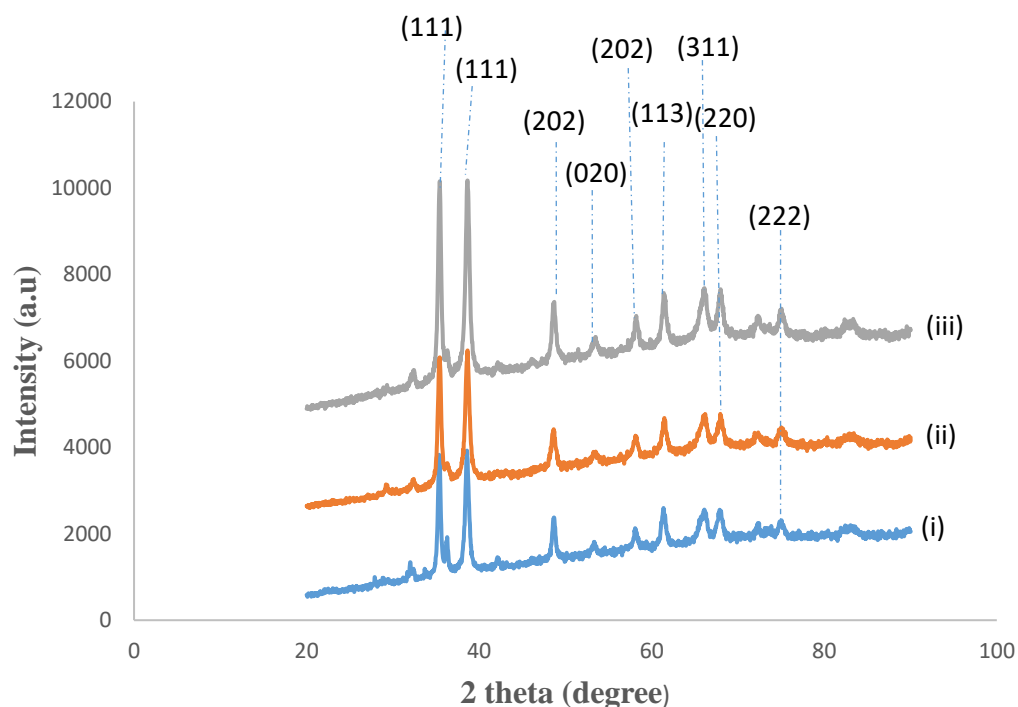
**Figure 7(c):** X-ray Diffraction of CuO Nanoparticles calcined at 500°C for (i) 1 h (ii) 2 h and (iii) 3 h.

Generally, it was observed from the XRD pattern in Figures 7 (a) – (c) that, as the calcination temperature and holding time increased from (300°C to 500°C) for 1 to 3 hours, the peaks intensity increases especially the peaks with crystal planes (002) and (111) were much stronger than those of the other peaks observed in the XRD pattern. This suggests that the crystals were mainly dominated by the (002) and (111) peaks and the prepared material were crystalline in nature. The XRD spectra of the uncalcined CuO nanoparticles showed no apparent crystal peaks that correspond to any phase of CuO, which meant that the nanoparticle produced was amorphous instead of crystalline. It was observed that the average crystallite size of the synthesized nanoparticles calculated using the Scherrer's equation increased with increasing calcination temperature and holding time. This increase in crystallite size is an indication of the increase in crystallinity. This may be attributed to successful removal of the residual water from amorphous CuO nanoparticles (Ashwani *et al.*, 2013; Srivastava *et al.*, 2013). Thus, the calcined temperature and holding time plays a crucial role in the crystallization and particle size of the CuO. XRD graph of synthesized CuO nanoparticles using copper (II) chloride at different pH is shown in Figure 7 (d).



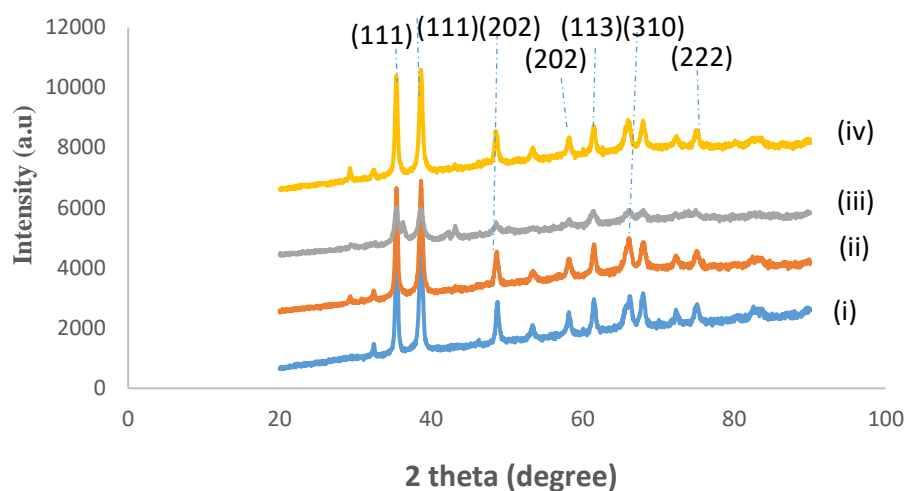
**Figure 7 (d):** XRD pattern of synthesized CuO nanoparticles using Copper (II) chloride at different pH (i) 7 (ii) 9 (iii) 11 (iv) 13.

XRD patterns of the CuO nanoparticle prepared at pH of 7, 9, 11 and 13 shown in Figure 7 (d) revealed the characteristics diffraction intense and sharp peaks at  $2\theta$  value of  $32.51^\circ$ ,  $35.54^\circ$ ,  $38.9^\circ$ ,  $38.7^\circ$ ,  $48.72^\circ$ ,  $53.49^\circ$ ,  $61.50^\circ$ ,  $66.5^\circ$ ,  $68.13^\circ$ ,  $75.25^\circ$  which were assigned to the following (110), (111), (200), (111), (202), (020), (113), (310), (220), (222) crystal planes respectively. The CuO nanoparticle prepared using copper (II) chloride at different pH corresponds to a typical monoclinic tenorite phase. It was observed that the intensity of diffraction peaks with crystal planes (110) and (111) reduced with increasing solution pH. This suggests that neutral pH did not favour successful growth of CuO nanoparticles compared to other pH values. The average crystallite size of CuO nanoparticles calculated using Scherrer formula was 9.9 nm, 5.82 nm, 10.89 nm and 5.86 nm for pH of 7, 9, 11 and 13 respectively. The crystallite sizes reported in this study is far smaller than 31-32 nm obtained by Topnani *et al.*, (2010) for CuO nanoparticles prepared using controlled wet soft method. The differences may be linked to the applied method of synthesis and other experimental conditions. XRD pattern of prepared CuO nanoparticles synthesized from copper sulphate at different pH is shown Figure 7 (e).



**Figure 7 (e):** XRD pattern of prepared CuO nanoparticles synthesized from copper sulphate at pH (i) 7 (ii) 9 (iii) 11.

According to Figure 7 (e), the XRD patterns of the CuO nanoparticle prepared at pH of 7, 9 and 11 demonstrated the characteristics and highly intense diffraction peaks at  $2\theta$  value of  $35.54^\circ$ ,  $38.7^\circ$ ,  $48.72^\circ$ ,  $53.48^\circ$ ,  $58.27^\circ$ ,  $61.53^\circ$ ,  $66.22^\circ$ ,  $68.13^\circ$ ,  $75.25^\circ$  which were assigned to (111), (111), (202), (020), (113), (310) crystal plane respectively. The CuO nanoparticle prepared using copper sulphate at different pH corresponds to a typical monoclinic tenorite phase. The average crystallite size of CuO nanoparticles calculated using Scherrer formula was 6.50 nm, 10.15 nm, 5.63 nm for pH of 7, 9 and 11 respectively. XRD analysis of CuO prepared from cupric acetate at different pH is shown in Figure 7 (f).



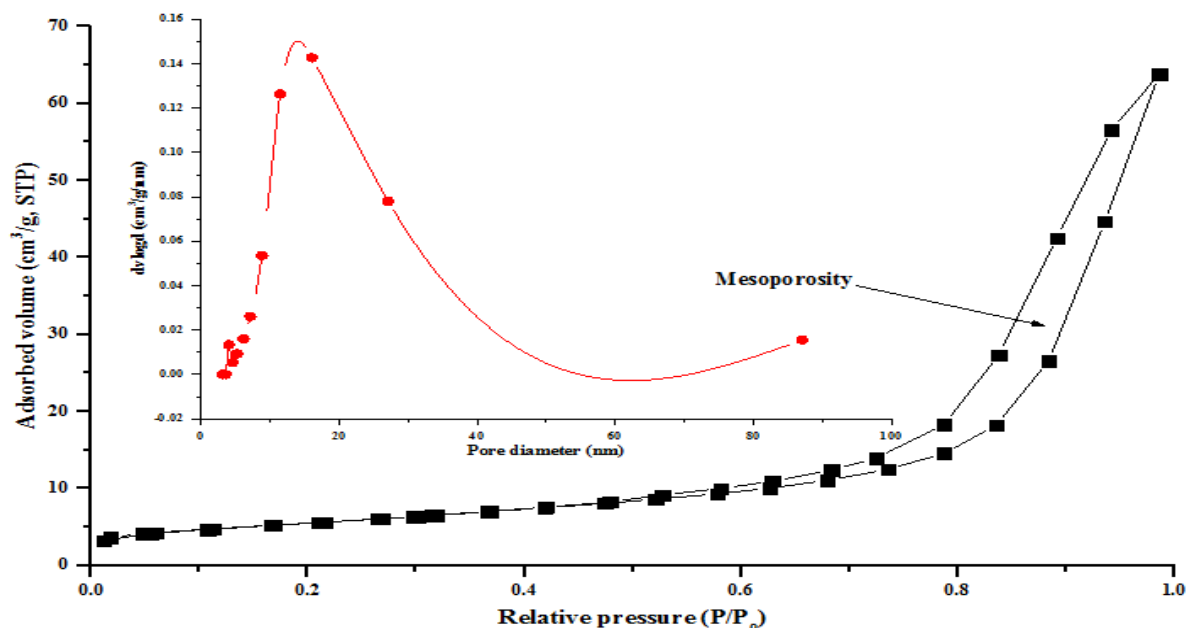
**Figure 7 (f):** XRD pattern of prepared CuO nanoparticles synthesized from cupric acetate at pH (i) 7 (ii) 9 (iii) 11 (iv) 13.

Figure 7 (f) revealed the formation of less intense but sharp diffraction peaks at  $2\theta$  value of  $35.54^\circ$ ,  $38.7^\circ$ ,  $48.72^\circ$ ,  $58.26^\circ$ ,  $61.52^\circ$ ,  $68.13^\circ$ ,  $75.25^\circ$  which were assigned to (111), (111), (202), (113), (310), (222) crystal plane respectively. The CuO nanoparticle prepared using cupric acetate at different pH corresponds to a typical monoclinic tenorite phase. The average crystallite size of CuO nanoparticles calculated using Scherrer formula was 5.72 nm, 5.37 nm, 6.00 nm and 6.74 nm for pH of 7, 9, 11 and 13 respectively. Compared to other copper salts precursor used, the intensities of diffraction peaks obtained using cupric acetate were low and may be attributed to the complex dissociation nature of the salt. Generally, it was noticed that irrespective of the calcinations temperature, holding time, solution pH and copper salt precursors, the CuO nanoparticles formed is pure and existed in single-tenorite phase with monoclinic structure (JCPDS-05-0661). The results obtained in this study closely agreed with the reported XRD patterns of CuO nanoparticles in the literature (Topnani *et al*, 2010). Thus, the optimum synthesis conditions for the preparation of Single-phase CuO nanoparticles with distinct spherical morphology were: solution pH 11, with copper sulphate salt precursor, and calcinations temperature and holding time of  $500^\circ\text{C}$  and 3 h respectively.

### **BET analysis of the synthesized CuO nanoparticles**

The surface area and pore size of the prepared sample was determined by Brunauer–Emmett–Teller (BET) technique. The  $\text{N}_2$  adsorption-desorption isotherms and the pore size

distribution of the sample based on Barrett–Joyner–Halenda (BJH) approach is depicted in Figure 8.

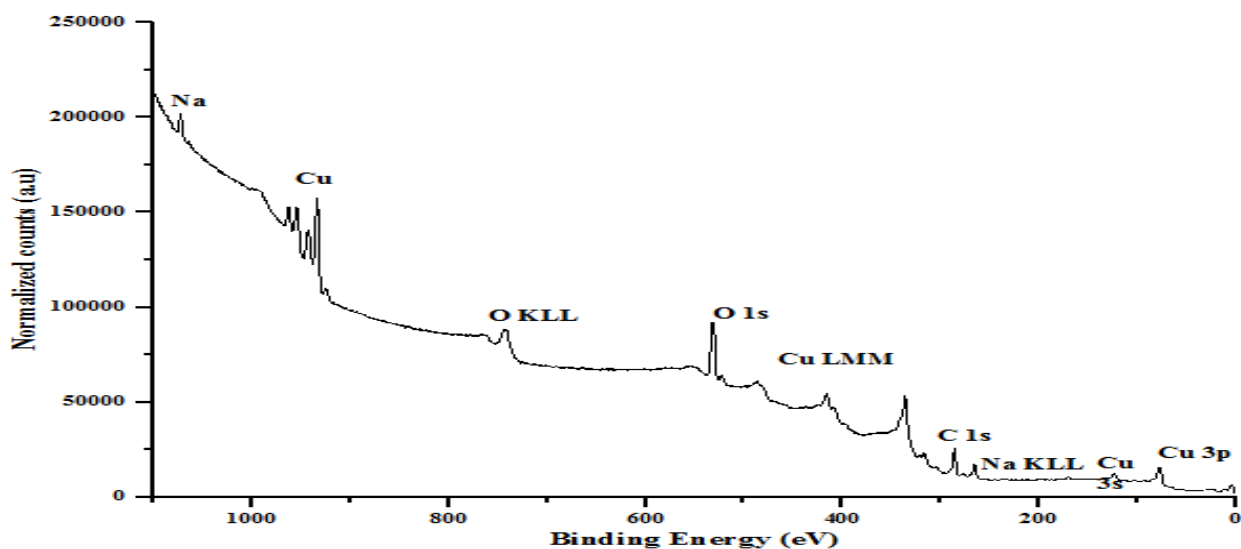


**Figure 8:** BET surface area and pore size distribution of CuO nanoparticles obtained at optimum conditions.

The BET surface area, pore volume and pore diameter of CuO nanoparticles was found to be 20.64 m<sup>2</sup>/g, 0.080 cc/g and 11.51 nm. According to IUPAC, the prepared material is mesoporous in nature and belongs to hysteresis loop type IV which further supports the result obtained from HRSEM analysis in Figure 7 (c). The hysteresis loop was small at low pressure and increase at a relative high pressure, which is an indication of increase in BET surface area. The pore size and pore shaped distribution in H3 hysteresis type is small and may be linked to the plant extract addition during the synthesis. These smaller mesopores is as a result of the interstices between primary crystallites. The BET surface area reported in this study is however greater than 15.6931m<sup>2</sup>/g obtained by Ren *et al.* (2009) who prepared CuO nanoparticles via thermal plasma technology. The formation of material with much higher surface area is an indication of more active catalytic sites. Topnani *et al.* (2010) reported surface area of 1.3 m<sup>2</sup>/g for CuO nanoparticles prepared using controlled non-aqueous sol-gel method. This is far smaller than 20.64 m<sup>2</sup>/g obtained in this study and the differences may be ascribed to the method of synthesis and type of the copper salt precursor used

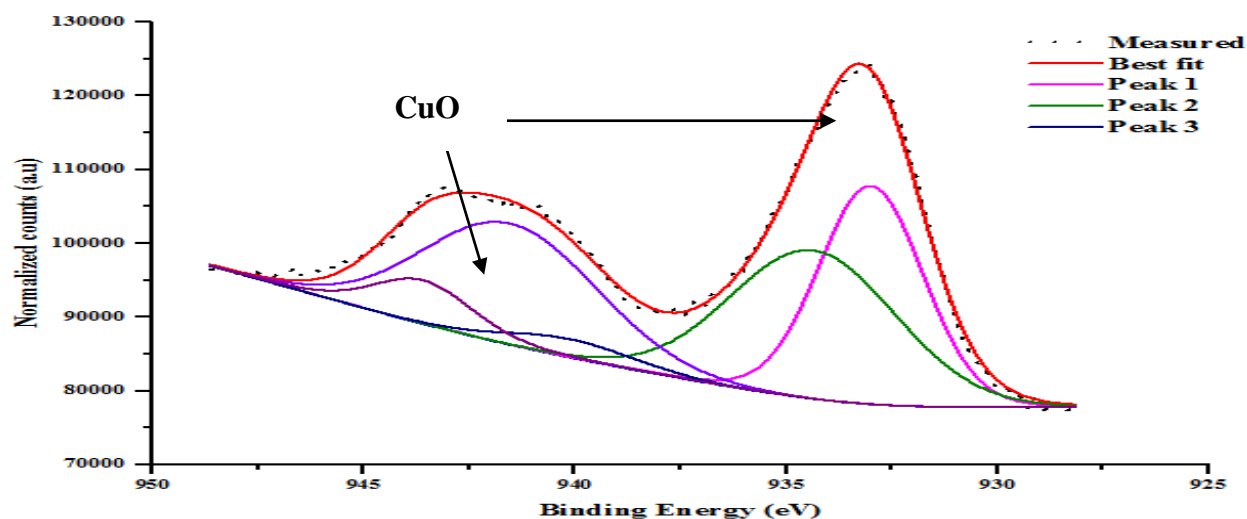
**XPS analysis of the prepared CuO nanoparticles**

Figure 9 shows the XPS general survey of the dominant elements on the surface of CuO nanoparticles. As can be seen from the spectra, XPS survey of CuO revealed the presence of Cu, O and C at different binding energies.



**Figure 9:** XPS general survey of the prepared CuO nanoparticles.

While Figure 10 represents the high resolution scan of Cu 2p core level and revealed the presence of two dominant peaks located at binding energies of 933 eV and 943.6 eV, which corresponds to the Cu 2p<sub>3/2</sub> only and further corroborated the existence of Cu in the +2 valence state. The data reported in this study match well for the Cu 2p orbital in CuO.



**Figure 10:** High resolution XPS spectrum of Cu  $2p_{3/2}$  peak.

Furthermore, additionally occurrence of three shakeup satellite peaks in the binding energies of 934.4 eV, 940.1 eV, 941.6 eV further confirmed that the Cu is a monotype (CuO) and not divalent ( $\text{Cu}_2\text{O}$ ). These values were however 1.4 eV, 7.1 eV, 8.6 eV greater in binding energy than the main peak noticed at 933 eV. Most of the fits were within 0.1 eV to the positions reported by Biesinger *et al.*, (2010) and Suleiman *et al.* (2010). Not only that, the shape and energy positions are unmistakably that of CuO. Additionally, the O 1s core-level spectrum shown in Figure 11 revealed the presence of four dominant peaks at different binding energies.

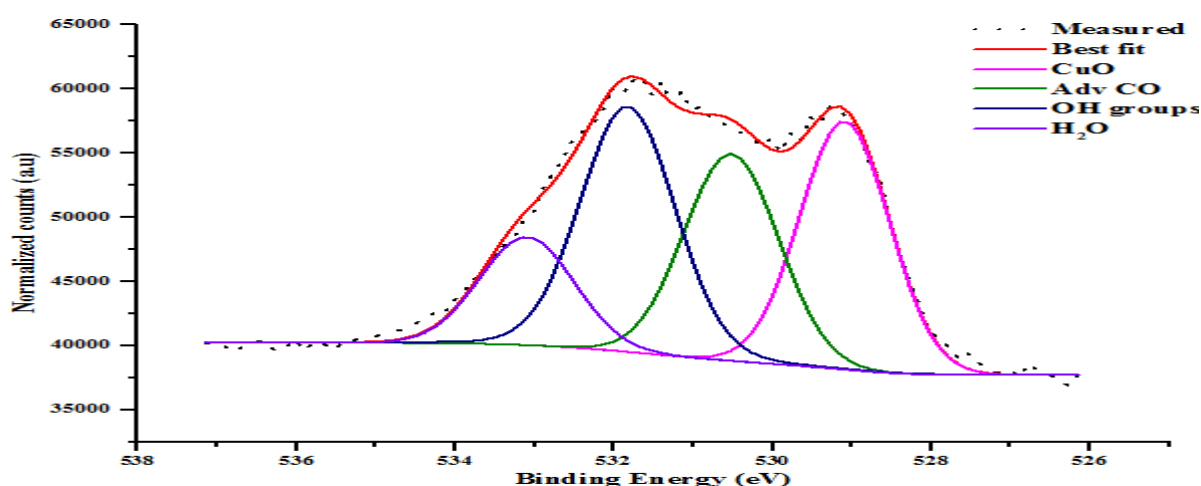


**Figure 11.** High resolution XPS spectrum of O 1s core-level spectrum.

The sharp peak observed at binding energy of 529.09 eV, correspond to oxygen in 2-oxidation state while the peak noticed at 531.37 eV, was ascribed to adsorbed oxygen on the surface of the CuO particles. The peak at 531.37 eV can be assigned as C=O and C-O groups and originated from the carboxylate groups in the plant extract used for the synthesis. The presence of carbonaceous species in the XPS spectra further suggests that the prepared material was actually carbon doped CuO nanoparticles. The other two peaks at the binding energies of 532.68 eV and 533.95 eV on the surface of the nano-CuO particles were linked to OH groups and H<sub>2</sub>O respectively. The formation of several strong shake-up satellites in sample further showed the Cu in the synthesized material exist in 2+ and not +1 oxidation state as in the case of Cu<sub>2</sub>O. The XPS result is in agreement with the XRD pattern which revealed that the prepared material is a single-phase CuO.

#### 4. Conclusion

CuO nanoparticles were successfully synthesized via biosynthetic route using *Khaya senegalensis* plant extract and different copper salt precursors at different solution pH. The CuO nanoparticles were subjected to different calcination temperatures and holding time and the characterization results showed that the materials were highly crystalline with spherical morphology and exist in a single tenorite phase. The characterization results revealed that calcination temperature, holding time, solution pH and copper salt precursors exhibited drastic effects on the formation and crystallization of CuO nanoparticles. It was established that calcination temperature of 500°C and holding time of 3 h, solution pH 11 using only copper sulphate salt produced spherical CuO nanoparticles with most distinct and intense peaks.

#### References

- Alabi, A.B., Coppede, N., Vilani, M., Calestani, D., Zappetini, A., Babalola, O.A. and Salvatore, I. (2013): Photocatalytic activity of nanostructured copper(II) oxide particles. *Ife Journal of Science*. **15**(2), 409-414.
- Ansilin, S., Nair, K. J., Aswathy, C., Rama, V., Peter, J. and Jeyachynthaya, P. J. (2016): Green synthesis and characterization of copper oxide nanoparticles using *Azadirachta indica* (Neem) Leaf Aqueous Extract. *Journal of Nanoscience and Technology*. **2**(5), 221-223.

- Ashwani, S., Sanjay, K., Narender, B., Sanjay, D. and Mohan, S. (2013): Effects of Calcination on Optical Properties and Morphology of NiO-CuO Nanocomposite. *Scholars Research Library*. **5**(3), 122-128.
- Asemani, M. and Anarjan, N. (2019): Green synthesis of copper oxide nanoparticles using *Juglans regia* leaf extract and assessment of their physico-chemical and biological properties. *Green Process Synthesis*. **8**, 557–567.
- Anwaar, S., Maqbool, Q., Jabeen, N., Nazar, M., Abbas, F., Nawaz, B., Hussain, T. and Hussain, S. Z. (2016): The effect of Green Synthesized CuO Nanoparticles on Calluslogenesis and Regeneration of *Oryza sativa* L. *Frontiers in Plant Science*. **7**, 1330-1 – 1330-9.
- Biesinger, M. C., Lau, L. M. W., Gerson, A. R. and Smart, R. S. C. (2010): Resolving surface chemical states in XPS analysis of first row transition metals, oxides and hydroxides: Sc, Ti, V, Cu and Zn. *Applied Surface Science*. **257**, 887–898.
- Das, D., Nath, B. C., Phukon, P. and Dolui, S. K. (2013): Synthesis and Evaluation of Antioxidant and Antibacterial Behavior of CuO Nanoparticles. *Colloids and Surfaces B: Biointerfaces*. **101**, 430-433
- Devasenan, S., Hajara, N. and Jayanthi, S. S. (2016): Synthesis and Characterization of Copper Nanoparticles Using Leaf Extract of *Andrographis paniculata* and their Antimicrobial Activities. *International Journal of ChemTech Research*. **9**(4), 725-730.
- Etefagh, R., Azhir, E. and Shahtahmasebi, N. (2013): Synthesis of CuO nanoparticles and fabrication of nanostructural layer biosensors for detecting *Aspergillus niger* fungi. *Science Iranica*. **20**(3), 1055- 1058.
- Ghorbani, H. R. (2014): Chemical synthesis of Copper nanoparticles. *Oriental Journal of Chemistry*. **30**(2), 803-806.
- Jaise, M. G., Arun, A. and Beena, M. (2018): Metal oxide nanoparticles in electrochemical sensing and biosensing. *Microchimica Acta*. **185**, 358-368.
- Jayalakshmi A, and Yogamoorthi, A., (2014): Green synthesis of copper oxide nanoparticles using aqueous extract of flowers of *Cassia alata* and particles characterization. *International Journal of Nanomaterials and Biostructures*. **4**(4), 66-71.
- Joshua, P. J., Krishnan, S., Vidhya Raj, D. J., Uthrakumar, R., Laxmi, S. and Jerome Das, S., (2014): Novel synthesis of tenorite (CuO) nanoparticles by wet chemical method. *International Journal of ChemTech Research*. **6**(3), 2002-2004.

- Katwal, R., Kaur, H., Sharma, G., Naushad, M. and Pathania, D. (2015): Electrochemical synthesis copper oxide nanoparticles for enhanced photocatalytic and antimicrobial activity. *Journal of Industrial and Engineering Chemistry*. **31**, 173-184.
- Koshi, J. and George, K. C. (2014): Annealing effects on crystallite size and band gap of CuO nanoparticles. *International Journal of Material Physics*. **5**(1), 35-42.
- Li, X., Xu, H., Chen, Z. S. and Chen, G. (2011): Biosynthesis of nanoparticles by microorganisms and their applications. *Journal of Nanomaterials*. **2011**, 1-16.
- Makarov, V. V., Love, A. J., Sinitsyna, O. V., Makarova, S. S., Yaminsky, I. V., Taliansky, M. E. and Kalinina, N. O. (2014): “Green” nanotechnologies: synthesis of metal nanoparticles using plants. *Acta Naturae*. **6**(1), 35-44.
- Naika, H. R., Lingaraju, K., Manjunath, K., Kumar, D., Nagaraju, G., Suresh, D. and Nagabhushana, H. (2015): Green synthesis of CuO nanoparticles using *Gloriosa superba* L. extract and their antibacterial activity. *Journal of Taibah University for Science*. **9**, 7-12.
- Othmane, A., Younes, E., Aziz, F., Mohamed, L. and Mohamed, Z. (2017): Effect of calcination temperature on the structure and catalytic performance of copper-ceria mixed oxide catalysts in phenol hydroxylation. *RSC Advances*. **7**, 12586-12597.
- Outokesh, M., Hosseinpour, M., Ahmadi, S. J., Mousavand, T., Sadjadi, S. and Soltanian, W. (2011): Hydrothermal synthesis of CuO nanoparticles: study on effects of operational conditions on yield, purity, and size of the nanoparticles. *Industrial and Engineering Chemistry Research*. **50**, 3540-3554.
- Padil, V. V. T. and Černík, M. (2013): Green synthesis of copper oxide nanoparticles using gum karaya as a biotemplate and their antibacterial application. *International Journal of Nanomedicine*. **8**, 888-898.
- Phiwdang, K., Suphankij, S., Mekprasart, W. and Pecharapa, W. (2013): Synthesis of CuO nanoparticles by precipitation method using different precursors. *Energy Procedia*. **34**, 740-745.
- Ren, G., Hu, D., Cheng, E. W. C., Vargas-Reus, M. A., Reip, P. and Allaker, R. B. (2009): Characterisation of copper oxide nanoparticles for antimicrobial applications. *International Journal of Antimicrobial Agents*. **33**, 587–590
- Saied, T. F and Ali, R. (2016): Green Synthesis and Characterization of Copper Oxide Nanoparticles using Coffee Powder Extract. *Journal of Nanostructures*. **6** (2), 160-164.

- Salem, E. T. Fakhry, M. A., Hassen, H. (2013): Metal oxide nanoparticles for optoelectronic devices fabrication. *International Journal for Nanoelectronics and Materials*. **6**(2), 121-128.
- Sharma, J. K., Akhtar, M. S., Ameen, S., Srivastava, P. and Singh, G. (2015): Green synthesis of CuO nanoparticles with leaf extract of *Calotropis gigantea* and its dye-sensitized solar cells applications. *Journal of Alloys and Compounds*. **632**, 321-325
- Siddiqui, H., Qureshi M. S. and Haque Z. (2016): Effect of copper precursor salts: Facile and sustainable synthesis of controlled shaped copper oxide nanoparticles. *Optik-International Journal for Light and Electron*. **127**(11), 4726-4730
- Srivastava, S., Mahendra, K., Arvind, A. and Sudhanshu, K. D. (2013): Synthesis and Characterization of Copper Oxide Nanoparticles. *IOSR Journal of Applied Physics*. **5**(4), 61-65.
- Suleiman, M., Mousa, M., Hussein, A., Hammouti, B., Hadda, T. B. and Warad, I. (2013): Copper (II)-oxide nanostructures: synthesis, characterization and their applications-reviews. *Journal of Materials and Environmental Science*. **4**(5), 792-797.
- Sumitha, S., Vidhya, R. P., Lakshmi, S. M. and Prasad, K. S. (2016): Leaf Extract Mediated Green Synthesis of Copper Oxide Nanoparticles Using *Ocimum tenuiflorum* and its Characterization. *International Journal of Chemical Science*. **14** (1), 435-440.
- Thi, T. V., Rai, A. K., Gim, J. and Kim, J. (2014): Potassium-doped copper oxide nanoparticles synthesized by solvothermal method as an anode material for high-performance lithium ion secondary battery. *Applied Surface Science*. **305**, 617-625.
- Topnani, N, Kushwaha, S. and Athar, T. (2010): Wet Synthesis of Copper Oxide Nanopowder. *International Journal of Green Nanotechnology: Materials Science and Engineering*. **1**(2), M67-M73.
- Umar, A., Rahman, M. M., Al-Hajry, A. and Hahn, Y. B. (2009): Ultra-sensitive cholesterol biosensor based on low-temperature grown ZnO nanoparticles. *Electrochemical Community*. **11**, 278–281
- Zhang, L., Yuan, F., Zhang, X. and Yang, L. (2011): Facile synthesis of flower like copper oxide and their application to hydrogen peroxide and nitrite sensing. *Chemistry Central Journal*. **5**(75), 220-227.
- Zhou, Y., Lin, W., Huang, J., Wang, W., Gao, Y., Lin, L., Li, Q., Lin, L. and Du, M. (2010): Biosynthesis of Gold Nanoparticles by Foliar Broths: Roles of Biocompounds and Other Attributes of the Extracts. *Nanoscale Research Letters*. **5**(8), 1351-1359.